JGR Atmospheres

RESEARCH ARTICLE
10.1029/2025JD044509

More Frequent and Intense Tropical Cyclone-Heat Wave Compound Extremes Over the Coastal Regions of China in a Warmer Climate

Pinya Wang[1,2], Cuini Qi[1,2], Yang Yang[1,2], Lili Ren[3], Jianping Tang[4], and Hong Liao[1,2]

[1]State Key Laboratory of Climate System Prediction and Risk Management/Jiangsu Key Laboratory of Atmospheric Environment Monitoring and Pollution Control/Jiangsu Collaborative Innovation Center of Atmospheric Environment and Equipment Technology/Joint International Research Laboratory of Climate and Environment Change, Nanjing University of Information Science and Technology, Nanjing, China, [2]School of Environmental Science and Engineering, Nanjing University of Information Science and Technology, Nanjing, China, [3]College of Environment and Ecology, Jiangsu Open University, Nanjing, China, [4]School of Atmospheric Sciences, Nanjing University, Nanjing, China

Abstract In recent decades, the tropical cyclone (TC) and heat wave (HW) (TC-HW) compound extreme event poses increasing threats to population over southeastern coast of China (SECC) under climate warming, yet their future projection remains uncertain. This study examines the projected changes in frequency, intensity, and spatial patterns of TC-HW events over the SECC using observational data and high-resolution climate model simulations from the Coupled Model Intercomparison Project Phase 6 (CMIP6) High-Resolution Model Intercomparison Project (HighResMIP). Based on the CMIP6 HighResMIP simulations, TC-HW events are projected to be more frequent and much stronger in the future under the high-emission scenario (SSP-585). Specifically, tropical cyclones (TCs) induce prelandfall warming over the SECC land region, particularly over the eastern part, with magnitude exceeding 1.5°C relative to the summertime climatology for 1980–2010. Such prelandfall warming associated with TC is driven by subsidence and increased solar radiation, followed by postlandfall cooling with temperature anomalies reaching up to −1°C relative to the historical summertime climatology. In the future, the model projections indicate that TC-HW events will be stronger, with temperature exceedance above 2°C, relative to the historical summertime climatology. Besides, TC-HWs are also expected to be more frequent, with the annual occurrences projected to increase by 30–50 events compared with the historical period. Our analysis reveals that the projected increases in TC-HWs are predominantly driven by the enhanced frequency and intensity of HWs under global warming. Moreover, TC-HWs will exhibit broader spatial extent of influence as well as the prolonged durations even from TC genesis stages. These findings underscore the increasing risks of compound TC-HW extremes in coastal China under the warming climate. Strengthening early warning systems and implementing urban heat mitigation strategies are critical to address these escalating threats.

Plain Language Summary Tropical cyclones (TCs) and heat waves (HWs) are two types of extreme weather events that can severely affect coastal populations. Observational analyses show that these two extremes have an increasing tendency to occur in close succession, forming compound TC-HW events whose impacts can be even more devastating. In this study, we examine how these compound events might change in the future over southeastern coastal China, a densely populated and vulnerable region. Using observational data and high-resolution climate model simulations from CMIP6 HighResMIP, we find that compound TC-HW events are projected to become more frequent and significantly stronger under a high greenhouse gas emission scenario (SSP5-8.5). Such increases in TC-HWs are primarily attributed to background warming, which favors more frequent and intense HWs, thereby increasing the likelihood of their cooccurrence with TCs. These events are expected to cause temperature increases of more than 2°C than the summertime climatology for a historical period and a prolonged duration. Our findings highlight the growing threat of compound extremes in a warming climate and the urgent need for improved early warning systems and urban heat mitigation strategies.

Key Points:

- Tropical cyclones (TCs) cause prelandfall warming in southeastern coastal of China (SECC), leading to tropical cyclone-heat waves (TC-HWs)
- Multimodel simulations from CMIP6 HighResMIP reasonably reproduce the observed TC-HWs characteristic over SECC during historical period
- Under SSP5-8.5 scenario, TC-HW events over SECC are projected to become more frequent and intense, based on CMIP6 HighResMIP simulations

Supporting Information:

Supporting Information may be found in the online version of this article.

Correspondence to:

Y. Yang,
yang.yang@nuist.edu.cn

Citation:

Wang, P., Qi, C., Yang, Y., Ren, L., Tang, J., & Liao, H. (2025). More frequent and intense tropical cyclone-heat wave compound extremes over the coastal regions of China in a warmer climate. *Journal of Geophysical Research: Atmospheres*, *130*, e2025JD044509. https://doi.org/10.1029/2025JD044509

Received 4 JUN 2025
Accepted 10 NOV 2025

Author Contributions:

Conceptualization: Pinya Wang
Formal analysis: Cuini Qi
Funding acquisition: Yang Yang
Methodology: Pinya Wang
Resources: Yang Yang
Supervision: Yang Yang
Visualization: Cuini Qi
Writing – original draft: Pinya Wang
Writing – review & editing: Pinya Wang, Cuini Qi, Yang Yang, Lili Ren, Jianping Tang, Hong Liao

1. Introduction

Tropical cyclones (TCs) are among the deadliest and most destructive natural disasters, causing substantial socioeconomic and infrastructural damage (Patricola & Wehner, 2018). For instance, Typhoon Haiyan (2013) resulted in over 6,300 deaths (Lagmay et al., 2015) and $4.5 ~ 5.1 billion in the Philippines (Delforge et al., 2025).

TC is most active in the western North Pacific (WNP), which accounts for nearly one-third of the global TCs (Lee et al., 2012). Consequently, the densely populated coastal regions of China are particularly susceptible to TC-related disasters, including storm surges, floods, and coastal erosion (Li et al., 2023; Needham et al., 2015; Xi et al., 2025). Moreover, TCs are a leading cause of large-scale power outages, with landfalling storms often causing extensive damage to electrical grids, leading to prolonged restoration times and posing significant risks to public safety (Feng et al., 2022).

Recent decades have witnessed a marked intensification of TCs globally, a trend largely attributed to rising sea surface temperatures since the mid-1970s (e.g., Carstens et al., 2025). These stronger storms tend to persist longer and exhibit greater destructive potential (Kossin et al., 2020; Li et al., 2023), amplifying risks in vulnerable coastal areas. The annual mean lifetime peak intensity of landfalling TCs in East and Southeast Asia has intensified by 12%–15% since the late 1970s, mainly contributed by a rise in the Category 4–5 storms (Mei & Xie, 2016). Since the 1980s, the WNP basin has experienced substantial multidecadal variability in TC activity, marked by shifts in both frequency and intensity (Kossin et al., 2020; Murakami et al., 2020). Furthermore, since the 1980s, TCs have undergone a robust poleward migration in their lifetime-maximum-intensity (LMI) latitudes locations—at rates of 53 ± 43 km decade^{-1} in the Northern Hemisphere and 62 ± 48 km decade^{-1} in the Southern Hemisphere (Studholme et al., 2022). In addition, TC translation speeds have decreased globally by 10% from 1949 to 2016, elevating the risk of extreme local rainfall (Kossin, 2018). Overall, these trends underscore the growing threat of TCs, exacerbating the risks associated with TCs (Lai et al., 2020; Utsumi & Kim, 2022).

On the other hand, recent decades have seen a robust increase in HWs across most land regions, with anthropogenic greenhouse gas forcing identified as the dominant driver of more frequent and severe HWs (Allan et al., 2021). Observational data and attribution studies show that summer HWs in China have become more frequent, more intense, and longer lasting (Wang et al., 2017) and are projected to further intensify under continued climate warming (Wang et al., 2023). In addition to anthropogenic forcing, internal climate variability, such as changes in the western Pacific subtropical high and the El Niño–Southern Oscillation, can modulate the spatial patterns and severity of HWs in China (Adhikari & Wang, 2025; Liu et al., 2019).

The compound hazard of TCs and HWs has been a growing concern. Notably, Matthews et al. (2019) proposed the TC-heat wave compound hazard and demonstrated a worldwide tendency for TCs to cause warming prior to landfall. This foundational work highlights the significant compound risk when intense TCs trigger widespread power outages, which critically impair air conditioning functionality. Such synergistic effects may lead to mortality and morbidity rates far exceeding those from either disaster alone (Santos-Lozada & Howard, 2018; Wu et al., 2022). Building upon this, subsequent studies have further investigated the mechanisms and impacts of TC-HW events (Chang et al., 2024; Guido et al., 2022; Zhang et al., 2024). For instance, Zhang et al. (2024) found that TCs can induce HWs through their peripheral downdrafts, which suppress cloud formation and precipitation, allowing intense solar radiation to reach the surface. Concurrently, adiabatic warming from subsiding air coupled with reduced humidity and localized Foehn effect, amplifies surface temperatures. Guido et al. (2022) noted heat anomalies typically peak within 3 days following a TC's passage, with the most pronounced anomalies occurring several days poststorm. Additionally, prior to landfall, TCs can exacerbate HWs by strengthening regional subtropical high-pressure systems (Wang et al., 2023). Over the past 60 years, the frequency of TC-HW compound events in the southeastern coast of China (SECC) has been steadily increasing, alongside a continuous rise in their proportion relative to all HWs events (Wang et al., 2023).

Under global warming, the frequency and severity of HWs across the world are projected to increase significantly (Brown, 2020; Perkins-Kirkpatrick & Lewis, 2020; Wang et al., 2019). Concurrently, TC activity in the WNP is anticipated to shift, with a projected decrease in overall TC frequency but an increase in the proportion of high-intensity TCs (Cha et al., 2020). These evolving trends highlight a growing need regarding the projected TC-HW compound extremes over the densely populated WNP region. However, accurately forecasting and predicting TC activity remains a major challenge due to significant uncertainties, particularly related to the coarse spatial resolution of climate models. These uncertainties, in turn, limit confidence in projections of future TC-HW compound events. Wu et al. (2022) utilized a dynamically downscaled Coupled Model Intercomparison Project Phase 5 (CMIP5) model with a 25-km resolution under the Representative Concentration Pathway 4.5 (RCP4.5) scenario, finding that their runs still tend to underestimate peak TC intensity. This may be attributable to biases in physical parameterizations of the climate model, resulting in substantial uncertainty in projections of compound events. To address these deficiencies, the use of a multimodel ensemble with high global resolution

and improved physical parameterizations is essential for improving the representation of TC-HW events and enhancing the reliability of future projections.

In this study, we aim to project the future changes in the frequency, intensity, and spatial distributions of compound TC-HWs over the SECC, a highly vulnerable region to both TCs and HWs during the summer season (Qi et al., 2024; Wang et al., 2023). Although previous studies have advanced our understanding of TC-HW compound events, there remain significant uncertainties in future projections due to the limitations of coarse-resolution models and the sensitivity to different TC-tracking algorithms. To address these deficiencies, we used observational records of air temperatures and TC tracks, reanalysis data sets of key meteorological parameters, and three available high-resolution climate models participating in CMIP6 HighResMIP. These models cover both a historical period (1980–2010) and a future projection period (2015–2050) and are paired with two TC-tracking algorithms. To assess model uncertainty, we compare the performance of different models and TC detection methods in simulating and identifying TCs. This study offers preliminary insights into the future changes of compound TC-HWs over the SECC region. The remainder of the paper is organized as follows: Section 2 presents the data sets and methodology; Section 3 presents the analyses of the future changes in key feathers of the TC-HW compound extremes over the SECC; and Section 4 provides the concluding remarks and discussion.

2. Data and Methods

2.1. Observed and Reanalysis Data Sets

For observational TC tracks, we use six-hourly best track data during 1980–2010, secured from the National Meteorological Information Centre of China Meteorological Administration (CMA). This data set includes the time, location, and intensity of TCs and records all of TCs that have passed through the WNP since 1949 (Lu et al., 2021; Ying et al., 2014). Observed daily maximum temperature from grid CN05.1 is utilized, which incorporates site observations in more than 2000 stations covering mainland China at a 0.25° × 0.25° resolution (Wu & Gao, 2013).

Meteorological parameters include 2-m air temperature (T2m), meridional winds (uwnd), zonal winds (vwnd), mean sea level pressure (MSLP), surface solar radiation downward (SSRD), and vertical velocity at 500 hPa from the fifth generation of the European Centre for Medium-Range Weather Forecasts (ECMWF) reanalysis data (ERA5), which is the latest global atmospheric reanalysis of ECMWF (Hersbach et al., 2020). The temporal resolution for each meteorological parameter is 6 hr, which are all utilized to generate daily mean values. All meteorological data were subsequently averaged to daily means for further analysis. In this study, ERA5 reanalysis data were extracted for the southeastern coastal region of China (105°–118°E, 25°–30°N), and the data cover the historical period from 1980 to 2010.

2.2. CMIP6 Multimodel Simulations

The CMIP6 HighResMIP is a novel global climate model simulation experiment design (Haarsma et al., 2016), aimed at assessing the impact of horizontal resolution in climate models on simulation capability (Roberts et al., 2019). The simulations employed in our study were CMIP6 HighResMIP Tier 1 and Tier 3, which are specifically known as the highresSST-present and highresSST-future experiments (Haarsma et al., 2016). The Tier 1 atmospheric-only simulation was driven by daily observed 0.25° sea surface temperature (SST) and sea ice concentration (SIC) data from 1950 to 2014, with radiative forcing and other settings identical to those used in the CMIP6 historical simulations (Eyring et al., 2016). The Tier 3 simulation was an extension of the Tier 1 to 2050 forced by SST and SIC data from Shared Socioeconomic Pathways 585 (SSP5-8.5) scenario (Haarsma et al., 2016). SSP5-8.5 is a fossil fuel-intensive development pathway, with the highest greenhouse gas emissions, leading to a radiative forcing of about 8.5 W/m^2 by 2100 and global warming of ~4.4°C (likely range 3.3–5.7°C) relative to preindustrial levels (IPCC, 2021). In this work, the storm tracks are derived from model simulations involved in the HighResMIP, accessible through the Earth System Grid Federation (ESGF). Specifically, we use three available models involved in HighResMIP, including CNRM-CM6-1-HR (hereafter CNRM; Voldoire et al., 2019), HadGEM3-GC31-HM (HadGEM; Roberts et al., 2019), and EC-Earth3P-HR (EC-Earth3P; Haarsma et al., 2020). Among these models, CNRM-CM6-1-HR has a higher resolution (approximate 0.5°), while EC-Earth3P-HR and HadGEM3-GC31-HM have a higher resolution of approximately 0.35° or less.

In addition, we use two distinct storm tracking algorithms to identify the storm track, that is, TRACK and TempestExtremes. TempestExtremes identifies sea level pressure minima with closed contours of pressure that satisfy a warm-core criterion based on the geopotential height difference between 500 and 300 hPa (Ullrich et al., 2021; Ullrich & Zarzycki, 2017). TRACK works by converting the output from each model to a standardized T63 spectral grid, where spectral filtering helps eliminate noise from the smallest spatial scales of vorticity. It then identifies vorticity maxima, defined as values greater than 5×10^{-6} s^{-1}, at each time step, and connects these maxima using a nearest-neighbor method (Hodges et al., 2017). The Centre for Environmental Data Analysis provides TCs and extratropical cyclones that have been identified through "TRACK" and "TempestExtremes" storm tracking algorithms.

To identify TC activity in the three models, we apply two widely used storm tracking algorithms, TempestExtremes and TRACK, to the model outputs for the historical period (1980–2010) and the future period (2015–2050). The identified tracks are then used to evaluate the models' ability to reproduce historical TCs and to project future changes in TC-HW compound events. To ensure the independence between the historical period (1980–2010) and the future scenario period (2015–2050), the years 2011–2014 were designated as a model transition and validation period and were excluded from the main trend analysis. Moreover, meteorological parameters in multimodels including daily maximum near-surface air temperature (tasmax), eastward_wind (uas), northward_wind (vas), and sea level pressure (psl) are used for analyses.

2.3. Identifications of TC-HW Compounds

The SECC region has experienced a significant increasing trend in both the frequency and intensity of heat waves around the mid-1980s (Wang et al., 2017; You et al., 2017). Additionally, the majority of TC tracks over the WNP have passed through the SECC region during their lifetimes in the past several decades (Wang et al., 2023). A heat wave day (heat wave (HW)) is defined as a day when the daily maximum temperature within the subregion of SECC (105°–118°E, 25°–30°N) (see the black box in Figure 5a) exceeds the 90th percentile of the seasonal distribution, which is obtained by pooling and ranking the reference period (1980–2010) samples. In this work, we classify all HWs into two categories: TC–heat waves (TC-HWs) and heat waves alone (AHWs). TC-HWs are defined when HWs occur over the land regions within the SECC, concurrent with the passages of TCs through the area, and AHWs indicate heat waves that occur independently. A topographic map of the SECC is shown in Figure S1 in Supporting Information S1. In this study, we focus on the future changes in frequency, intensity, and spatial distributions of TC-HWs during the summer season (June, July, and August) in the SECC.

In this work, the least squares method is applied to fit the linear trend, and the Pearson correlation coefficient was used to quantify the linear relationship between variables.

3. Results

3.1. Evaluation of CMIP6 Multimodel Simulated Tropical Cyclones Under the Current Climate

The TC performance of the models in the historic period is assessed to give some context for the future changes. The temporal and spatial variations in the frequency of TCs observed between 1980 and 2010 in CMA is compared to the multimodel simulations processed by two storm tracking algorithms. During the historical period (1980–2010), observed records (Figure 1) reveal a decreasing trend in the frequency of TCs from 1980 to 2010 (−0.20 TCs/year, $p < 0.01$), which is consistent with the previous findings (Wang et al., 2023; Zhao et al., 2018). The simulated TC tracks in CNRM-CM6-1-HR and EC-Earth3P-HR exhibit an increasing trend from 1980 to 2010 while those simulated by the HadGEM3-GC31-HM align with the observational data, showing a decreasing trend. The multimodel ensemble mean (MME) can reduce the bias and uncertainty inherent in individual experiments (Chen et al., 2024) though it does not capture a statistically significant trend ($p > 0.1$). The analysis reveals that the multimodel ensemble mean processed with the TRACK storm-tracking algorithm is more consistent with the observational records, exhibiting a decreasing trend.

For a more in-depth assessment of model biases, we categorized the observed and simulated TCs into "landfalling" and "non-landfalling" events and conducted a detailed comparison of their interannual variations and long-term trends (Figure S2 in Supporting Information S1). This deeper evaluation reveals several important bias patterns. Regarding the number of landfalling TCs, the EC-Earth3P-HR model systematically underestimates the annual frequency when using the TempestExtremes algorithm; however, this negative bias is considerably

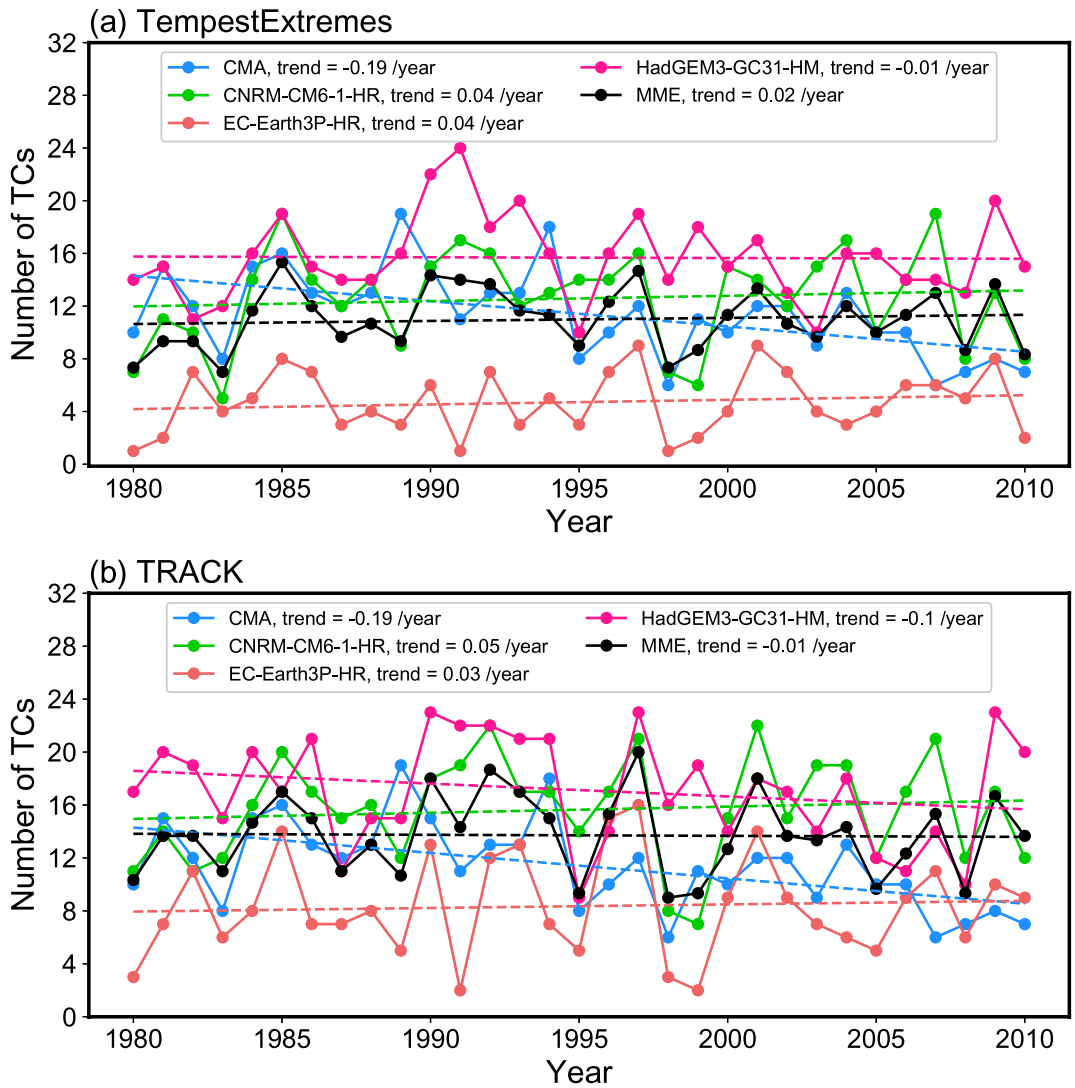

Figure 1. The interannual variations of tropical cyclone frequency during the summer season (June, July, and August) from 1980 to 2010 using (a) TempestExtremes and (b) TRACK storm tracking algorithms. The results from three individual models and the ensemble mean are presented. The observational results are denoted by the blue line. All analyses are based on the regional mean within the southeastern coastal of China domain (105°–118°E, 25°–30°N).

ameliorated when the TRACK algorithm is applied. A more critical finding relates to the simulation of long-term trends. Observational data show a significant decreasing trend in the frequency of landfalling TCs from 1980 to 2010. Models using the TempestExtremes algorithm universally failed to capture the significant decreasing trend in the frequency of landfalling TCs observed from 1980 to 2010, instead simulating an opposing positive trend. In contrast, a key result is that when the TRACK algorithm is used, the MME and several individual models successfully reproduce a decreasing trend consistent with observations. This comparative analysis therefore highlights the decisive impact of the TC-tracking algorithm choice on model evaluation outcomes and suggests that the TRACK algorithm, in conjunction with the high-resolution models, provides more reliable results for simulating the climatological trends of landfalling TCs relevant to this study.

Regarding spatial patterns, the multimodel simulations successfully reproduced the observed high-frequency regions of TCs over the SECC for the historical period (1980–2010). Individual models achieved spatial correlation coefficients above 0.7 with observational data, while the multimodel ensemble mean (MME) correlation exceeded 0.8, demonstrating a high level of fidelity in capturing the key spatial characteristics of TCs (Figures 2 and 3).

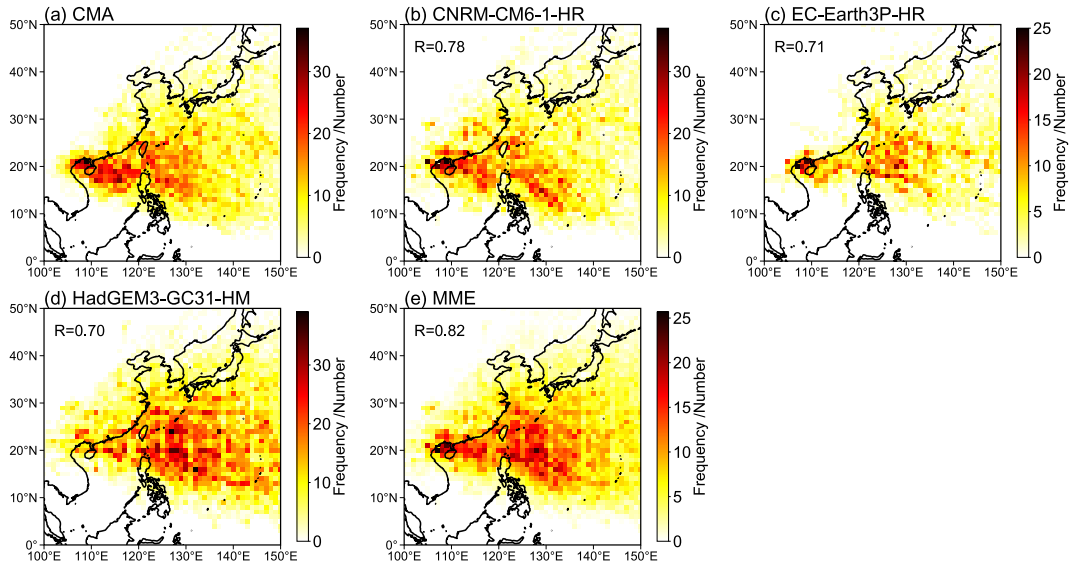

Figure 2. Spatial distribution of the frequency of tropical cyclones derived from the TempestExtremes storm-tracking algorithm during the summer season from 1980 to 2010. Panel (a) presents the observed results, panels (b)–(d) display outputs from three individual models, and panel (e) shows the model ensemble mean.

In addition to the frequency and spatial distribution, the ability of models to simulate TC intensity is another critical aspect of model evaluation. We categorize the wind speeds based on the intervals marked in Figure 4, which align with standard TC classifications: Interval 1 corresponds to tropical storms (TS, 17.2–24.4 m/s), Interval 2 to severe tropical storms (STS, 24.5–32.6 m/s), Interval 3 to typhoons (TY, 32.7–41.4 m/s), Interval 4 to severe typhoons (STY, 41.5–50.9 m/s), and Interval 5 represents supertyphoons (SuperTY, ≥51.0 m/s).

Based on this classification, the observational data (CMA, black line) show a primary peak frequency within Interval 1 (TS), indicating that most TCs have a relatively low to moderate intensity. A secondary, smaller peak is also noticeable in Interval 3 (TY). A key point of consistency is that all models, despite quantitative differences,

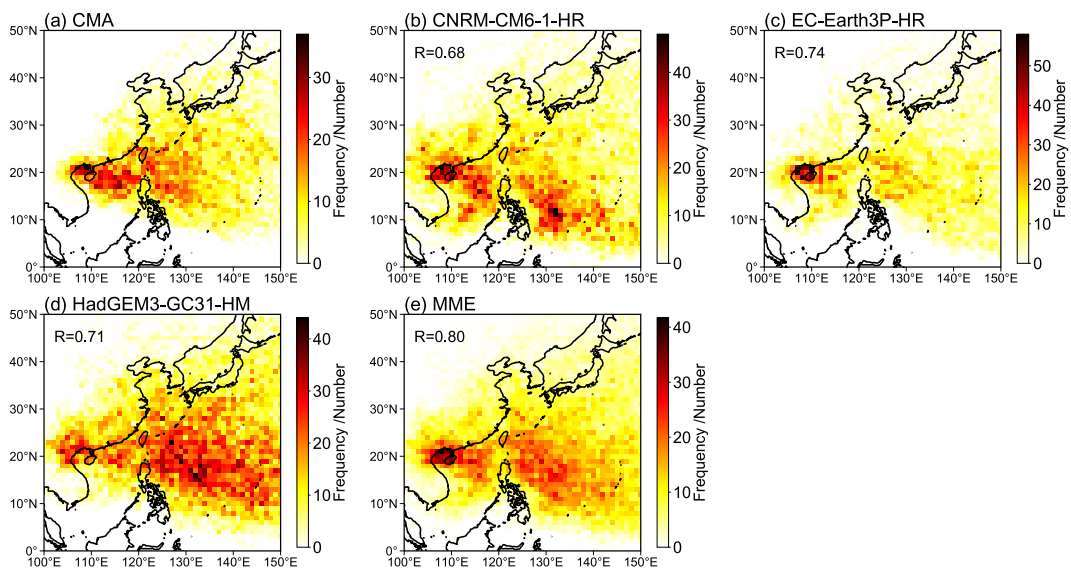

Figure 3. Spatial distribution of the frequency of tropical cyclones derived from the TRACK storm-tracking algorithm during the summer season from 1980 to 2010. Panel (a) presents the observed results, panels (b)–(d) display outputs from three individual models, and panel (e) shows the model ensemble mean.

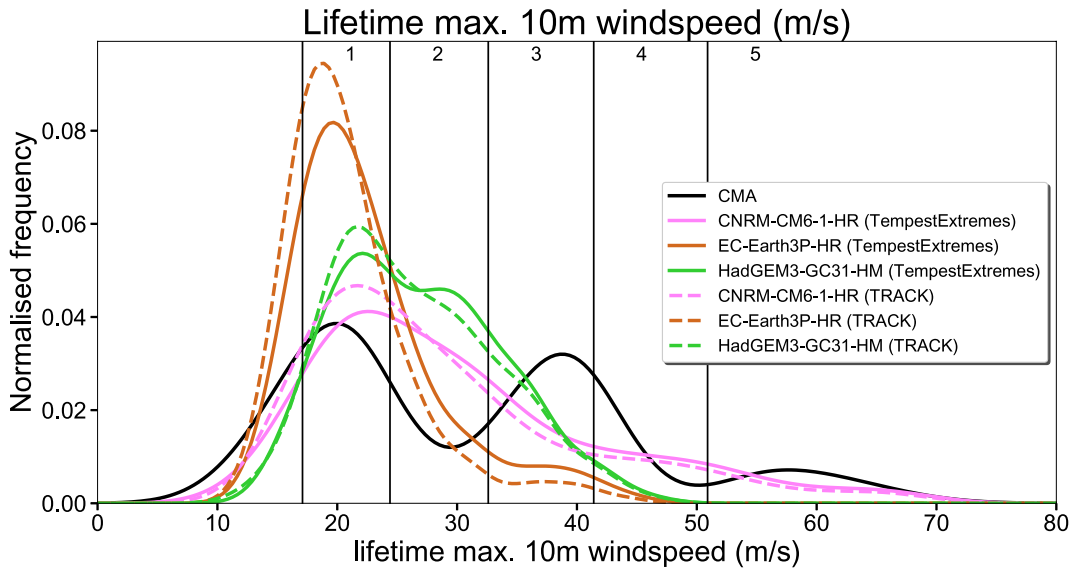

Figure 4. The normalized frequency distribution of lifetime maximum 10m wind speed for tropical cyclones during the summer season (1980–2010). The black line represents observational data. Colored lines show the simulation results from different CMIP6 HighResMIP models, where the solid and dashed lines correspond to the TempestExtremes and TRACK storm tracking algorithms, respectively. The vertical lines numbered 1–5 indicate wind speed thresholds for reference.

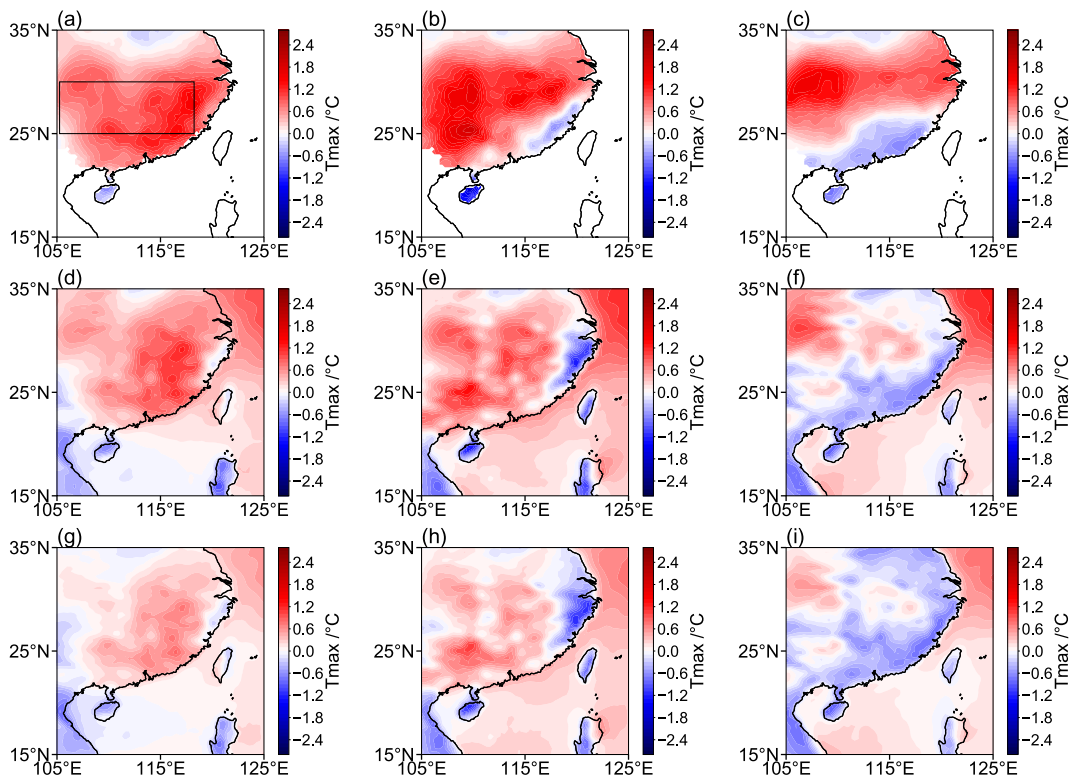

Figure 5. The spatial distribution of the composite anomalies of daily maximum temperature relative to the summer climatology during the three days prelandfall (a, d, and g), landfall day (b, e, and h), and three days postlandfall (c, f, and i) periods for tropical cyclones from 1980 to 2010. Panels (a)–(c) are based on observational data from the China Meteorological Administration. Panels (d)–(f) and (g)–(i) are based on the TempestExtremes and TRACK storm tracking algorithms, respectively. For TempestExtremes and TRACK, anomalies represent the ensemble mean of three models. Prelandfall and postlandfall anomalies were averaged over the respective 3-day windows.

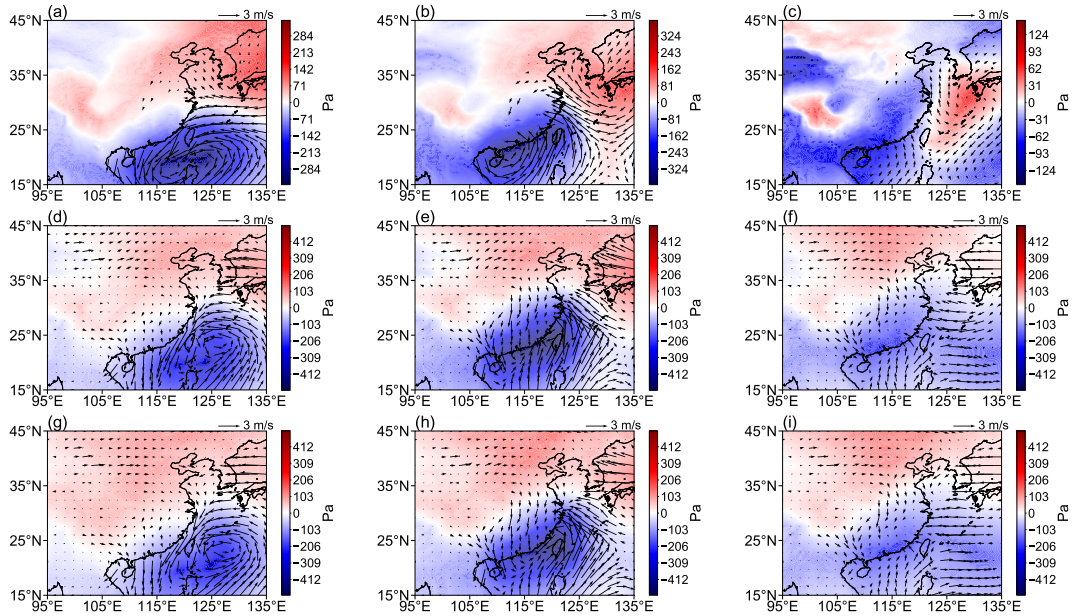

Figure 6. Same as in Figure 5, but for the anomalous of surface-level pressure and 10-m winds.

successfully reproduce this fundamental trend by also showing their highest frequency peak in Interval 1. This demonstrates a shared ability to capture the general characteristic that weaker storms are the most common.

However, distinct biases are also evident. For instance, the HadGEM3-GC31-HM model (both TRACK- and TempestExtremes-based results) exhibits a positive bias, with its peak frequency shifted into Interval 2 (STS), suggesting a tendency to simulate stronger TCs on average. In contrast, the EC-Earth3P-HR model, particularly when paired with the TRACK algorithm (gray line), shows a distribution peak that aligns well with the observations in Interval 1. The most significant and common deficiency across nearly all models is the underestimation of the frequency of the most intense TCs. This is particularly evident in the right tail of the distribution, corresponding to Intervals 4 (STY) and 5 (SuperTY), where all model-simulated frequency curves lie significantly below the observational curve. Such biases in simulating TC intensities of global climate models are consistent with previous work, likely driven by coarse horizontal resolution (Knutson et al., 2020) and uncertainties in physics parameterization schemes, particularly those governing convection and boundary layer processes (Reed & Jablonowski, 2011).

3.2. Variations of Meteorological Variables Over the SECC Land Region Before and After Tropical Cyclone Landfall

This study analyzes the composite anomalies of daily maximum T2m (T_{max}), MSLP, and 10-m wind speed relative to the summertime climatology in the three days before and after TC landfall during the historical period, aiming to explore the effects of TC landfalls on meteorological environments dominating the SECC.

The meteorological analysis for the historical period (1980–2010) reveals significant prelandfall warming across most of the SECC land area, particularly in the eastern regions, where temperatures increase by over 1.5°C (Figure 5a). This phenomenon may be attributed to two main factors. First, the enhanced southeasterly winds associated with the outer circulation of the TC transport warm and moist air to the eastern part of the SECC land area (Figure 6a). At the same time, the TC's outer circulation induces widespread and robust subsidence, as indicated by positive vertical velocity anomalies at 500 hPa over SECC landmass (Figure S3a in Supporting Information S1). This large-scale subsidence suppresses cloud formation, leading to clearer skies over the land. Consequently, a significant positive anomaly in SSRD is observed (Figure S4a in Supporting Information S1), indicating intense surface heating. Therefore, the combination of adiabatic warming from subsidence and strong diabatic heating from enhanced solar radiation acts as the dominant mechanism driving the formation of the prelandfall HW.

On the day of landfall, a noticeable cooling is observed in the immediate vicinity of the TCs (Figure 5b), while the majority of the region continues to experience temperature increases of approximately 2°C. Our analysis shows this localized cooling is caused by the TC's core, with its strong ascent and dense cloud cover, moving ashore, which sharply reduces incoming solar radiation (Figures S3b and S4b in Supporting Information S1). Following landfall, the southern part of the SECC undergoes substantial cooling, while central areas show a persistent warming trend (Figure 5c).

The simulated results from MME generally reproduced this observed pattern of prelandfall warming and postlandfall cooling (Figures 5d–5f & Figures 5g–5f). The simulated anomalies in daily maximum T2m from the TempestExtremes tracker demonstrate a high degree of consistency with the observed data (Figures 5d–5f). Specifically, prior to landfall, an increase in T2m is evident across most of the SECC (Figure 5d), accompanied by a substance-induced sea level pressure increase center (Figure 6d), yet it aligns more closely with TRACK results. On the day of landfall, significant cooling is seen in the eastern part of the SECC, with continued warming in the rest of the region (Figure 5e). As the cyclone dissipates postlandfall, cooling further intensifies in the southern regions, while central areas still experience warming (Figure 5f). Notably, the discrepancy in the location of the temperature anomalies between the model simulations and the observation could be attributed to model biases in cyclone tracking (Figure 2).

The results from the TRACK tracker (Figure 5g) indicate a less pronounced warming trend before landfall, with an average increase of about 0.5°C across the SECC, which is smaller in magnitude and more limited in extent than the observed data. On the day of landfall, significant cooling is observed in the eastern region of the SECC (Figure 5h), with both the intensity and extent of cooling larger than those in the observational data. Postlandfall, the area affected by cooling expands, and the cooling effect exceeds the observational results (Figure 5i).

A separate analysis of the three models processed by two TC trackers is performed, with Figure S5 in Supporting Information S1 displaying the results from TempestExtremes and Figure S6 in Supporting Information S1 presenting those from TRACK. The analysis indicates that in the TempestExtremes results, all three models accurately reproduce the temperature distribution prior to TC landfall. On the day of landfall, all models captured the locations of cooling and warming quite well. In the postlandfall phase, the CNRM-CM6-1-HR model showed closer agreement with the observations, whereas the EC-Earth3P-HR and HadGEM3-GC31-HM models overestimated the cooling regions. In contrast, the TRACK results reveal that all three models underestimated the warming region prior to landfall. On the day of landfall, the cooling regions in the CNRM-CM6-1-HR and HadGEM3-GC31-HM models were displaced toward the northeast relative to the observations, and in the postlandfall phase, all three models demonstrate substantial biases, markedly overestimating the cooling regions. In addition, TRACK and TempestExtremes algorithms show differences in the simulation of temperature anomalies, with TRACK generally producing larger cooling extents postlandfall than TempestExtremes.

3.3. The Observed and CMIP6 Simulated Frequency and Intensity of TC-HWs Under the Current Climate

Figure 7 illustrates the effects of TC trajectories on the frequency of extreme hot days over the SECC land areas during the historical period (1980–2010). The number of each grid point represents the occurrences of extreme hot days recorded over land when TCs are located at these positions, and that is the frequency of TC-HWs. China Meteorological Administration results indicate that the frequency of extreme hot days over the SECC land areas significantly increases when TCs approach the coast (Figure 7a), particularly when their centers are located within 110°–125°E and 15°–25°N.

The model simulations with the two TC algorithms, TempestExtremes and TRACK, exhibit discrepancies in both the spatial distribution and frequency of TC-HWs. Compared to TempestExtremes, the TRACK algorithm simulates a higher frequency and broader spatial coverage of TC-HWs over SECC land areas during TC passages. Simulations from the CNRM-CM6-1-HR model indicate that TCs originating from the southeastern direction and moving northeastward are more likely to trigger extreme hot days over SECC land areas (Figures 7b and 7f). Notably, when TC centers approach Hainan Island, the frequency of such events increases significantly, exceeding 30 times.

Results from the EC-Earth3P-HR model using the TempestExtremes algorithm indicates that the frequency of extreme hot days over land significantly increases when TCs approach Taiwan or Hainan Island (Figure 7c).

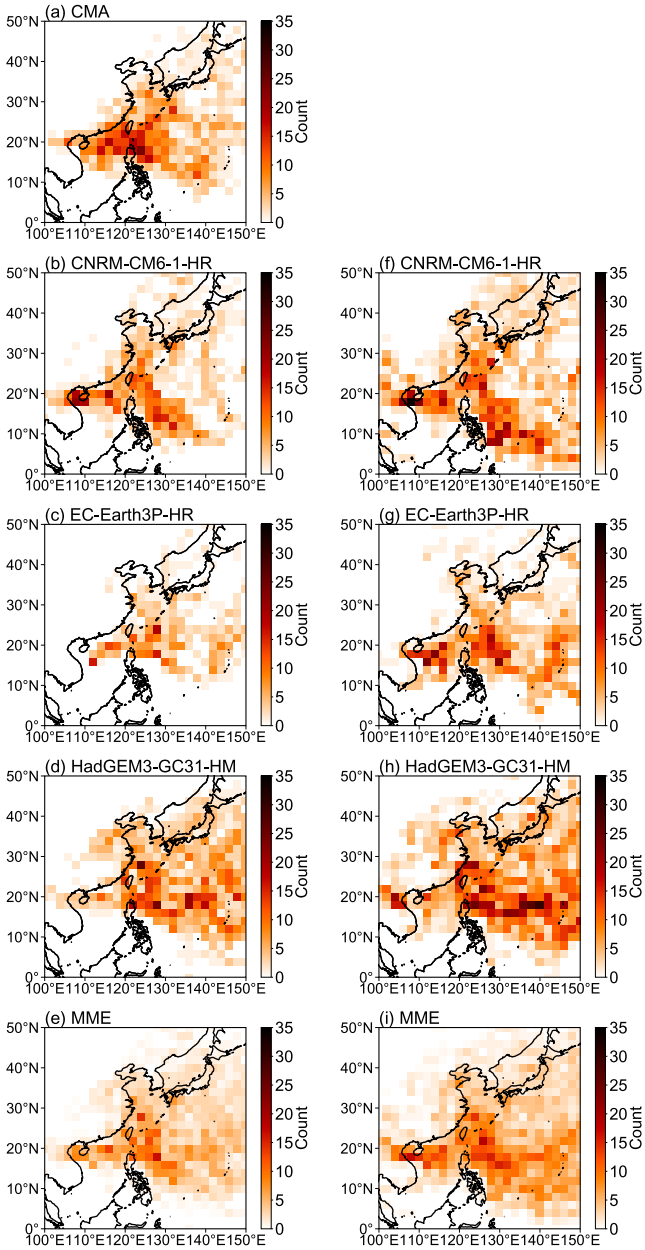

Figure 7. The spatial distribution of the frequency of extreme hot days in the southeastern coastal of China during the movement of tropical cyclones during the summer season from 1980 to 2010. Obtained from the (a) China Meteorological Administration observational results, (b)–(d) individual models using the TempestExtremes storm-tracking algorithm, (e) multimodel ensemble mean using TempestExtremes, (f)–(h) individual models using the TRACK storm-tracking algorithm, and (i) multimodel ensemble mean using TRACK.

However, compared to observational data, the model underestimates both the frequency and spatial extent of these extreme hot days. On the other hand, results from the EC-Earth3P-HR model processed with the TRACK method show that the frequency of extreme high-temperature events over land reaches its peak when TCs move within the region of 110°–130°E and 15°–25°N (Figure 7g), which is consistent with observational findings. Nevertheless, the spatial extent of extreme high-temperature events induced by TCs in the TRACK-based simulations is overestimated compared to observations.

The results from the HadGEM3-GC31-HM reveal a significant overestimation in the spatial distribution range of TC-HW frequencies (Figures 7d and 7h). Notably, both cyclone-tracking algorithms indicate consistent spatial patterns in the impact of TC trajectories on TC-HW frequencies, with the most pronounced effects concentrated in the 120°–140°E and the 15°–25°N region.

Compared with individual models, MME exhibits enhanced robustness and consistency (Figures 6i and 7e). Notably, analyses using two TC-tracking algorithms reveal spatially coherent patterns in the regions most affected by TC trajectories on the frequency of extreme high-temperature events over land (110°–135°E and 15°–30°N). However, both algorithms demonstrate a systematic overestimation in the spatial extent of these impacts.

Figure 8 illustrates the spatial distributions of the intensity of TC-HWs over the SECC during the historical period from 1980 to 2010. Each grid point represents the average temperature anomalies over land regions of SECC during hot extreme days accompanied by TC passages, relative to the summertime climatology, and that is the intensity of TC HWs. Observational results indicate that when TCs move near the Korean peninsula, the land Tmax over the SECC significantly increases, with a rise exceeding 2°C compared to the summer climatology (Figure 8a). When TCs are located far from land or are about to make landfall, the temperature increase during extreme hot days over the SECC is lower, with a warming amplitude of approximately 1°C than the summertime climatology.

Compared to observational results, the CNRM-CM6-1-HR model exhibits a significant overestimation of the intensity of TC-HWs over the SECC during the historical period (Figures 8b and 8f). Furthermore, the results processed by the TempestExtremes and TRACK methods show spatial consistency in this model. Specifically, when TCs are located over the ocean between Taiwan and northern Philippines or near the Korean peninsula, the temperature anomalies during TC-HWs are higher than those when TCs are at other locations, exceeding 2°C.

The simulation results of the EC-Earth3P-HR model show significant discrepancies compared to observational data (Figures 8c and 8g). Specifically, the model underestimates the intensity of TC-HWs near the Korean peninsula, while overestimating the intensity of TC-HWs around Taiwan Island. The simulation results of the HadGEM3-GC31-HM model exhibit an overestimation in the Yangtze River delta region (Figures 8d and 8h). However, consistent with observational data, the temperature during extreme hot days is higher when TCs are located near the Korean peninsula. Consistent with the observational results, the MME results show the higher temperature anomalies during TC-HWs when TCs are near the Korean peninsula, yet exhibiting a slight overestimation compared to the observations (Figures 8e and 8i).

In addition, during the historical period (1980–2010), observational data (CMA) already indicate a slight increasing trend (0.10 days/year) of TC-HW days in the SECC (Figure 9a), while the MME results more clearly

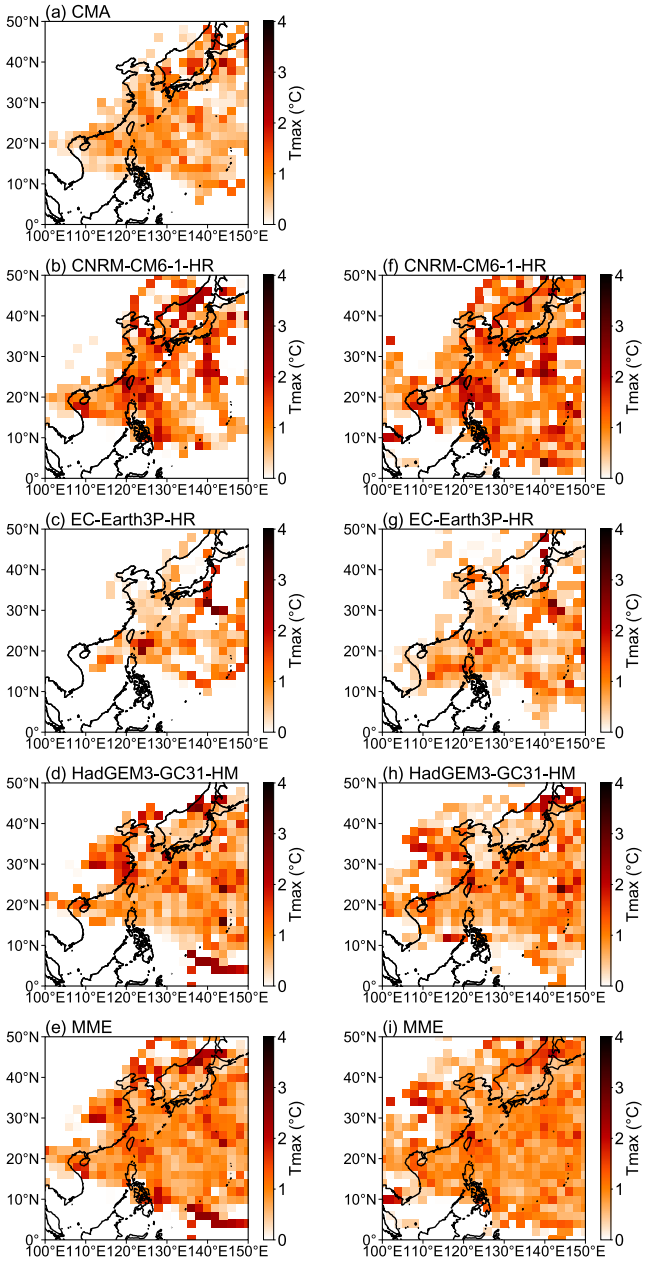

Figure 8. Average temperature anomalies during extreme hot days over southeastern coastal of China relative to the summer climatology, along with the movements of tropical cyclones during the summer season from 1980 to 2010. Obtained from the (a) China Meteorological Administration observational results, (b)–(d) individual models using the TempestExtremes storm-tracking algorithm, (e) multimodel ensemble mean using TempestExtremes, (f)–(h) individual models using the TRACK storm-tracking algorithm, and (i) multimodel ensemble mean using TRACK.

point to a significant increase, that is, 0.36 days/year for TempestExtremes and 0.39 days/year for TRACK. Both the observed and simulated increasing trends confirm that such events have indeed become more frequent (Figure 9).

3.4. The Projected Frequency and Intensity of TC-HWs in the Future

Under the future SSP5-8.5 scenario (2015–2050), TC-HW compound events are projected to become more frequent and more intense (Figures 10 and 11). The three climate models and their MME results reveal that TCs over the WNP in the future will cooccur with a significantly higher number of extreme hot days in the SECC land areas than the historical period (Figure 7). A comparison between the historical and future (Figure 10) simulations highlights this intensification that the peak occurrence count in the key hotspot regions (such as the South China Sea) is projected to approximately double, increasing from around 30–35 events over the historical period (1980–2010) to over 70 events for the future period (2015–2050). This stark increase in cooccurrence frequency is consistent with our main finding that background warming creates more frequent HW days, thereby increasing their probability of coinciding with TC passages. Furthermore, the projected interannual variations of TC-HWs for the 2015–2050 period under the SSP5-8.5 scenario suggest a significant acceleration in the growth trend relative the historical period. The MME projects an annual increase of 0.83 days/year for TempestExtremes and 1.05 days/year for TRACK (Figure S7 in Supporting Information S1), which substantially exceed their historical records. This indicates that compound TW-HW events will become more frequent in the future, at an accelerating rate.

The frequencies of simulated TC-HWs exhibit discrepancies across different climate models, yet the spatial distributions of hotspots derived from two TC algorithms show consistency for each model. Specifically, the CNRM-CM6-1-HR and EC-Earth3P-HR models indicate a significant increase in the frequency of TC-HWs over the SECC land areas when TCs traverse the oceanic region of 105°–115°E and 15°–20°N (Figures 10a and 10b and 10e–10F). In contrast, the HadGEM3-GC31-HM model systematically overestimates the frequency of TC-HWs, suggesting elevated extreme hot days occurrences over land when TCs are active within the broader latitudinal band of 15°–30°N (Figures 10c and 10g). Results with TempestExtremes detects TC-HWs prior to cyclone landfall, whereas extreme hot days over SECC land regions generally occur when TCs approach Hainan Island (Figures 10a–10c). The MME results effectively reconcile intermodel discrepancies and highlight robust features, demonstrating that TCs can induce extreme hot days in SECC land regions and a pronounced frequency increase in TC-HWs when TCs are within 10°–25°N (Figures 10d and 10h). Moreover, compared to the historical period, future TCs are projected to exert prolonged impacts on land extreme hot days. Under historical conditions, extreme hot days predominantly occurred during the immediate prelandfall phase; however, in future climate scenario, TCs may persistently influence land temperatures through remote dynamic-thermodynamic coupling from their genesis stage, potentially extending the duration of TC-HWs.

Significant discrepancies exist in the simulation results among different TC-tracking methods and across various models. All model simulations indicate that compared to the historical period, future TC-HWs over the SECC are projected to exhibit significantly stronger intensity with higher anomalies. Moreover, a broader range of TC tracks will trigger more intense extreme hot events, suggesting that the influence of TCs on terrestrial extreme heat may persist longer in the future. These prolonged effects of TCs on hot extremes is manifested both in terms of increased frequency and enhanced intensity of TC-HWs.

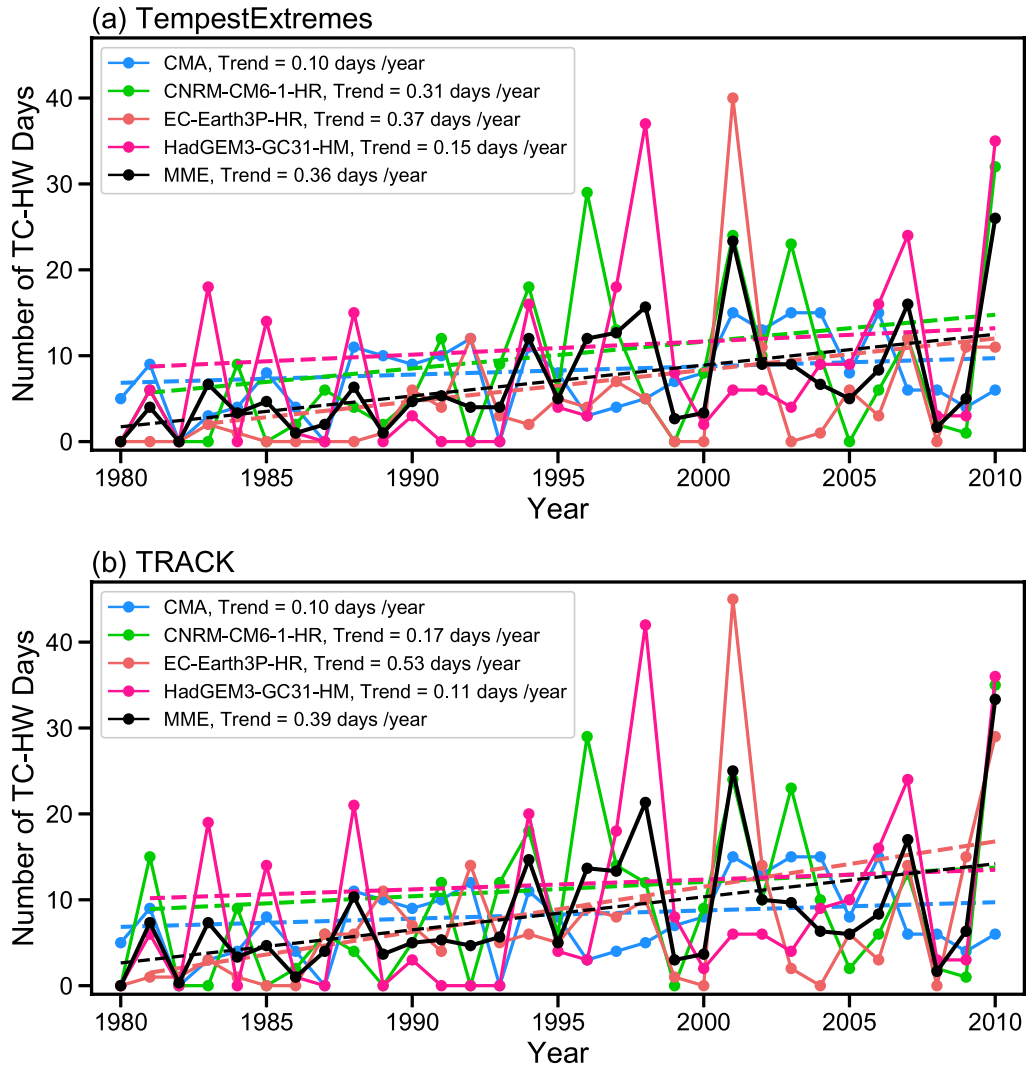

Figure 9. The interannual variations of tropical cyclone-heat wave frequency during the summer season (June, July, and August) from 1980 to 2010 using (a) TempestExtremes and (b) TRACK storm tracking algorithms. The results from three individual models and the ensemble mean are presented. The observational results are denoted by the blue line.

Although the EC-Earth3P-HR model systematically underestimates the intensity of TC-HWs compared to the CNRM-CM6-1-HR and HadGEM3-GC31-HM models, all three models consistently simulate similar spatial distributions patterns of TC-HWs (Figures 11a–11c and 11e–11g). Notably, when TC activity is located near the Korean peninsula and near the South China Sea, the simulated intensity of TC-HWs is apparently enhanced in all models.

In addition, we examine the changes in TC frequency and HW days separately. The results reveal that the annual total number of TCs does not show an increasing trend in either the historical or future periods; observational data even show a slight decrease historically (Figure S8 in Supporting Information S1). In contrast, the number of HW days shows a clear increase during the historical period (CMA: +0.24 days/year; MME: +0.27 days/year), a trend that is set to intensify in the future, with the MME projecting a growth rate of +0.88 days/year (Figure S9 in Supporting Information S1). Therefore, the long-term increase in the frequency of TC-HW is predominantly driven by the significant increase in HWs under global warming, rather than by changes in TC frequency.

To investigate the physical mechanisms behind the enhanced intensity of future TC-HW events and to distinguish the contribution of background warming from that of changes in the TC's dynamic and thermodynamic processes, we calculated the difference in Tmax between TC-HW and AHW events. Observational data (Figure S10a in

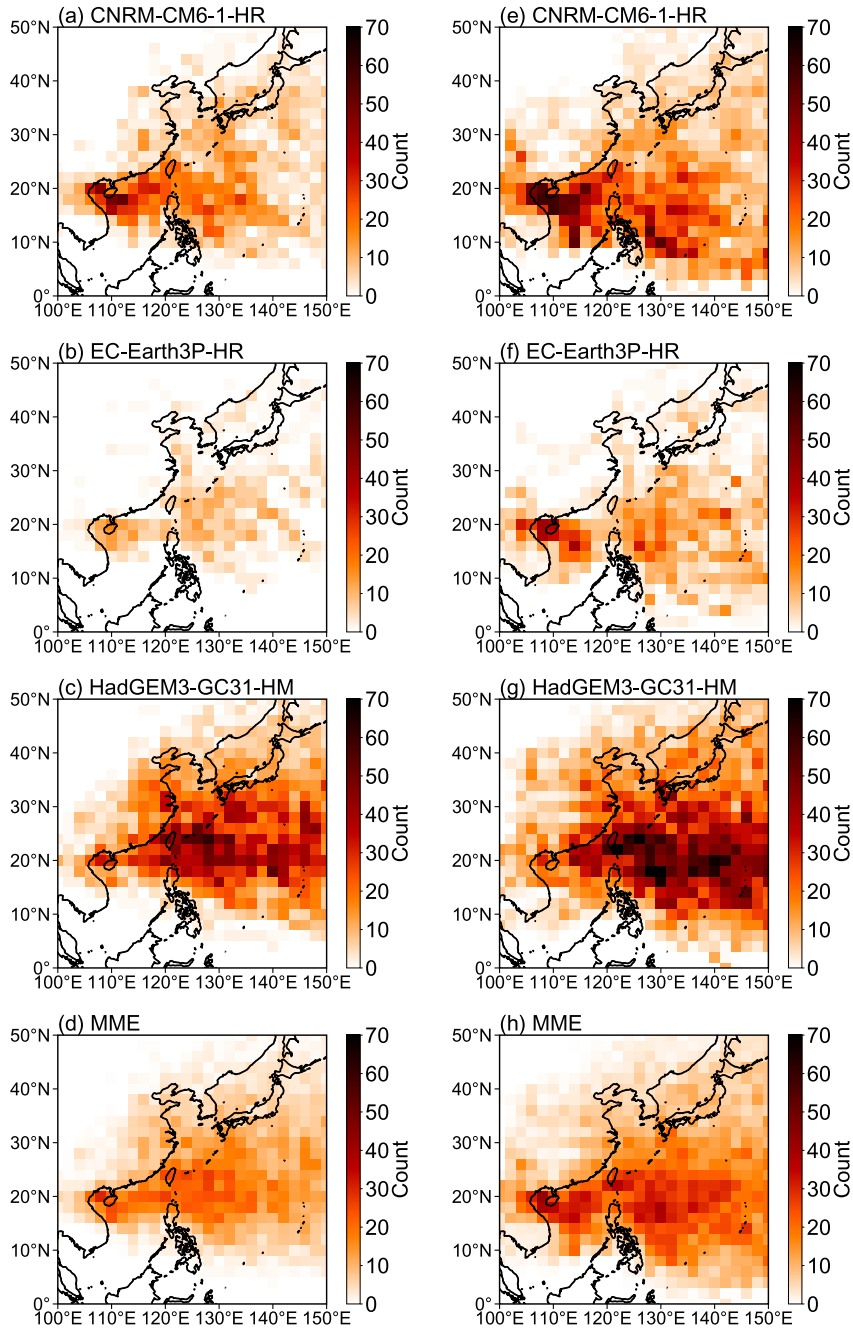

Figure 10. Projected spatial distribution of the frequency (total count) of extreme hot days associated with tropical cyclone movements over the southeastern coastal of China during the summer season from 2015 to 2050. Obtained from the (a)–(c) individual models using the TempestExtremes storm-tracking algorithm, (d) multimodel ensemble mean using TempestExtremes, (e)–(g) individual models using the TRACK storm-tracking algorithm, and (h) multimodel ensemble mean using TRACK.

Supporting Information S1) for the historical period (1980–2010) show that temperatures during TC-HW events were notably higher than during standalone heat waves in the northern and central parts of the SECC region, while being slightly lower in the northwestern and eastern coastal areas. Although some differences exist among the model simulations, all of them capture these regions of warming and cooling (Figures S10b–S10i in Supporting Information S1). This suggests that in the past climate, although the outer circulation of a TC could induce subsidence warming, this process may have also been accompanied by cooling effects from cloud cover or light

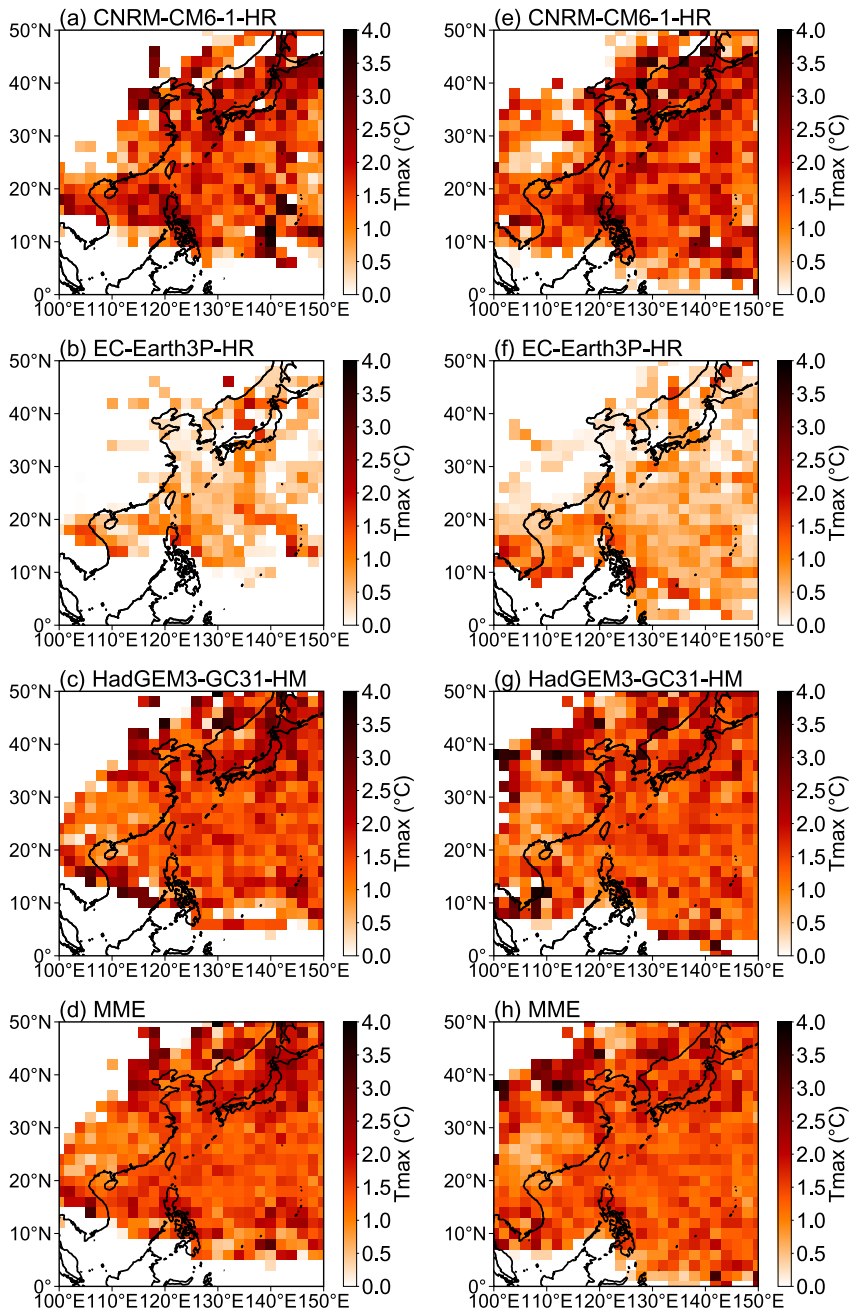

Figure 11. Average temperature anomalies during extreme hot days over southeastern coastal of China relative to the summer climatology, along with the movements of tropical cyclones during the summer season from 2015 to 2050. Obtained from the (a)–(c) individual models using the TempestExtremes storm-tracking algorithm, (d) multimodel ensemble mean using TempestExtremes, (e)–(g) individual models using the TRACK storm-tracking algorithm, and (h) multimodel ensemble mean using TRACK.

precipitation. The analysis for the future period reveals that this complex interaction is projected to continue. Model projections show that this heterogeneously spatial pattern is expected to persist (Figure S11 in Supporting Information S1). The MME results continue to show a spatially mixed pattern of positive and negative values without a widespread and strong warming signal. These results therefore indicate that the primary driver for the higher temperature anomalies observed in future TC-HW events is the background climate warming, which systematically elevates the baseline temperature of all HW events.

4. Summary and Discussions

This study assesses the observed and projected changes in frequency and intensity of TC-HWs over SECC based on observational records and multimodel simulations from CMIP6 HighResMIP. The results indicate that the frequency and intensity of TC-HW events will increase significantly under the future SSP5-8.5 scenario, which is consistent with the general expectation that global warming will exacerbate extreme events (IPCC, 2021). Our analysis further reveals that the fundamental driver of this trend is background climate warming, which systematically increases the probability and intensity of heat waves, thereby creating more favorable conditions for the formation of TC-HW events. In alignment with previous studies (Wang et al., 2023; Zhang et al., 2024), our analysis confirms that dynamic subsidence and enhanced solar radiation from reduced cloud cover, induced by the TC's outer circulation, are the key physical mechanisms driving prelandfall warming. Moreover, the persistent warming observed in some areas after a TC's passage is analogous to the findings of Guido et al. (2022), who noted that anomalous heat indices could last for several days post-TC landfalls.

Methodological choices, particularly the selection of the TC-tracking algorithm, constitute a primary source of uncertainty in this study. For instance, the choice between TC-tracking algorithms such as the vorticity-based TRACK and the pressure-based TempestExtremes significantly impacts the simulated temperature and pressure anomaly fields. This fundamental difference in detection criteria can lead to discrepancies in the identified storm tracks, frequency, and intensity, even when applied to the same model output. Although different trackers show some consistency in simulating TC spatial patterns, as noted by Horn et al. (2014) that for atmosphere-only simulations, spatial patterns of change are very similar across trackers despite large differences in detection rates, the design of the algorithms themselves (e.g., TRACK's use of multilevel vorticity averaging and warm-core criteria) may render it more sensitive and comprehensive. This might explain why TC trends simulated using TRACK align more closely with observations. This underscores the necessity of comparing different algorithms and interpreting their results with caution in such studies.

Furthermore, climate models possess inherent uncertainties. Despite employing state-of-the-art high-resolution models, a common deficiency across nearly all of them is the underestimation of the frequency of extremely intense TCs, such as supertyphoons. This systematic bias implies that our risk assessment for the most extreme and potentially most destructive future TC-HW compound events may still be conservative. Therefore, the current projections should be considered as a conservative, lower-bound estimate of future risk increases.

Conflict of Interest

The authors declare no conflicts of interest relevant to this study.

Data Availability Statement

The CN05.1 gridded temperature data are provided by the National Meteorological Information Center of the CMA, which can be obtained from Wu and Gao (2013). The best track data set of TCs is also released by CMA (Lu et al., 2021; Ying et al., 2014), which can be obtained by https://tcdata.typhoon.org.cn/zjljsjj_sm.html. The ERA5 reanalysis is available at https://cds.climate.copernicus.eu/ (Hersbach et al., 2023a; Hersbach et al., 2023b). The storm tracks derived from model simulations involved in the HighResMIP are accessible through the Earth System Grid Federation (ESGF, https://aims2.llnl.gov/search) data portals (World Climate Research Programme, 2019).

Acknowledgments
This study was supported by the National Key Research and Development Program of China (Grant 2024YFF0811400), the National Natural Science Foundation of China (Grants 42475032 and 42521006), and the Natural Science Foundation of Jiangsu Province (Grant BK20241902).

References

Adhikari, G. P., & Wang, G. (2025). Understanding the driving mechanism for heat waves variability over South Asia during El Niño and La Niña events. *Atmospheric Research*, *321*, 108076. https://doi.org/10.1016/j.atmosres.2025.108076

Allan, R. P., Hawkins, E., Bellouin, N., & Collins, B. (2021). IPCC, 2021: Summary for policymakers.

Brown, S. J. (2020). Future changes in heatwave severity, duration and frequency due to climate change for the Most populous cities. *Weather and Climate Extremes*, *30*, 100278. https://doi.org/10.1016/j.wace.2020.100278

Carstens, J. D., Uejio, C. K., Powell, E., Jung, J., & Zonka, S. (2025). Tropical cyclones and climate change: An overview for the public health community. *Environmental Research*, 122149. https://doi.org/10.1016/j.envres.2025.122149

Cha, E. J., Knutson, T. R., Lee, T.-C., Ying, M., & Nakaegawa, T. (2020). Third assessment on impacts of climate change on tropical cyclones in the typhoon committee region–part II: Future projections. *Tropical Cyclone Research and Review*, *9*(2), 75–86. https://doi.org/10.1016/j.tcrr.2020.04.005

Chang, Man-Hei, J., Lam, Y. F., Wong, Y.-C., & Hon, K. K. (2024). Compound tropical cyclone heat (TC-Heat) hazard in Hong Kong: Amplifying urban heat extremes with storm position-driven peripheral warming and urban footprint. *Journal of Geophysical Research: Atmospheres*, *129*(21), e2024JD041037. https://doi.org/10.1029/2024JD041037

Chen, K.-C., Hong, C.-C., Tsou, C.-H., & Wu, D.-R. (2024). Present climate and future changes in the annual cycle of TC activity in the WNP investigated by HighResMIP GCMs. *Journal of Climate*, *37*(18), 4775–4791. https://doi.org/10.1175/JCLI-D-24-0048.1

Delforge, D., Wathelet, V., Below, R., Lanfredi Sofia, C., Tonnelier, M., van Loenhout, J. A. F., & Speybroeck, N. (2025). EM-DAT: The emergency events database. *International Journal of Disaster Risk Reduction*, *124*, 105509. https://doi.org/10.1016/j.ijdrr.2025.105509

Eyring, V., Bony, S., Meehl, G. A., Senior, C. A., Stevens, B., Stouffer, R. J., & Taylor, K. E. (2016). Overview of the coupled model intercomparison project phase 6 (CMIP6) experimental design and organization. *Geoscientific Model Development*, *9*(5), 1937–1958. https://doi.org/10.5194/gmd-9-1937-2016

Feng, K., Ouyang, M., & Lin, N. (2022). Tropical cyclone-blackout-heatwave compound hazard resilience in a changing climate. *Nature Communications*, *13*(1), 4421. https://doi.org/10.1038/s41467-022-32018-4

Guido, Z., Allen, T., Mason, S., & Lázaro, P. M. (2022). Hurricanes and anomalous heat in the Caribbean. *Geophysical Research Letters*, *49*(21), e2022GL099740. https://doi.org/10.1029/2022GL099740

Haarsma, R., Acosta, M., Bakhshi, R., Bretonnière, P.-A., Caron, L.-P., Castrillo, M., et al. (2020). HighResMIP versions of EC-Earth: Ec-earth3p and EC-Earth3P-HR–Description, model computational performance and basic validation. *Geoscientific Model Development*, *13*(8), 3507–3527. https://doi.org/10.5194/gmd-13-3507-2020

Haarsma, R. J., Roberts, M. J., Luigi Vidale, P., Senior, C. A., Bellucci, A., Bao, Q., et al. (2016). High resolution model intercomparison project (HighResMIP v1.0) for CMIP6. *Geoscientific Model Development*, *9*(11), 4185–4208. https://doi.org/10.5194/gmd-9-4185-2016

Hersbach, H., Bell, B., Berrisford, P., Biavati, G., Horányi, A., Muñoz Sabater, J., et al. (2023a). ERA5 hourly data on pressure levels from 1940 to present [Dataset]. *Copernicus Climate Change Service (C3S) Climate Data Store (CDS)*. https://doi.org/10.24381/cds.bd0915c6

Hersbach, H., Bell, B., Berrisford, P., Biavati, G., Horányi, A., Muñoz Sabater, J., et al. (2023b). ERA5 hourly data on single levels from 1940 to present [Dataset]. *Copernicus Climate Change Service (C3S) Climate Data Store (CDS)*. https://doi.org/10.24381/cds.adbb2d47

Hersbach, H., Bell, B., Berrisford, P., Hirahara, S., Horányi, A., Sabater, J. M., et al. (2020). The ERA5 global reanalysis. *Quarterly Journal of the Royal Meteorological Society*, *146*(730), 1999–2049. https://doi.org/10.1002/qj.3803

Hodges, K., Cobb, A., & Vidale, P. L. (2017). How well are tropical cyclones represented in reanalysis datasets? *Journal of Climate*, *30*(14), 5243–5264. https://doi.org/10.1175/JCLI-D-16-0557.1

Horn, M., Walsh, K., Zhao, M., Camargo, S. J., Scoccimarro, E., Murakami, H., et al. (2014). Tracking scheme dependence of simulated tropical cyclone response to idealized climate simulations. *Journal of Climate*, *27*(24), 9197–9213. https://doi.org/10.1175/JCLI-D-14-00200.1

IPCC. (2021). Climate change 2021: The physical science basis. In V. Masson-Delmotte, P. Zhai, A. Pirani, S. L. Connors, C. Péan, S. Berger, et al. (Eds.), *Contribution of working group I to the sixth assessment report of the intergovernmental panel on climate change*. https://doi.org/10.1017/9781009157896

Knutson, T., Camargo, S. J., Chan, J. C. L., Emanuel, K., Ho, C. H., Kossin, J., et al. (2020). Tropical cyclones and climate change assessment: Part II: Projected response to anthropogenic warming. *Bulletin of the American Meteorological Society*, *101*(3), E303–E322. https://doi.org/10.1175/BAMS-D-18-0194.1

Kossin, J. P. (2018). A global slowdown of tropical-cyclone translation speed. *Nature*, *558*(7708), 104–107. https://doi.org/10.1038/s41586-018-0158-3

Kossin, J. P., Knapp, K. R., Olander, T. L., & Velden, C. S. (2020). Global increase in major tropical cyclone exceedance probability over the past four decades. *Proceedings of the National Academy of Sciences*, *117*(22), 11975–11980. https://doi.org/10.1073/pnas.1920849117

Lagmay, A. M. F., Agaton, R. P., Bahala, M. A. C., Briones, J. B. L. T., Cabacaba, K. M. C., Caro, C. V. C., et al. (2015). Devastating storm surges of typhoon Haiyan. *International Journal of Disaster Risk Reduction*, *11*, 2212–4209. https://doi.org/10.1016/j.ijdrr.2014.10.006

Lai, Y., Li, J., Gu, X., Chen, Y. D., Kong, D., Gan, T. Y., et al. (2020). Greater flood risks in response to slowdown of tropical cyclones over the Coast of China. *Proceedings of the National Academy of Sciences*, *117*(26), 14751–14755. https://doi.org/10.1073/pnas.1918987117

Lee, T. C., Knutson, T. R., Kamahori, H., & Ying, M. (2012). Impacts of climate change on tropical cyclones in the Western north Pacific basin. Part I: Past observations. *Tropical Cyclone Research and Review*, *1*(2), 213–235. https://doi.org/10.6057/2012TCRR02.08

Li, Y., Tang, Y., Li, X., Song, X., & Wang, Q. (2023). Recent increase in the potential threat of Western north Pacific tropical cyclones. *npj Climate and Atmospheric Science*, *6*(1), 53. https://doi.org/10.1038/s41612-023-00379-2

Liu, Q., Zhou, T., Mao, H., & Congbin, F. (2019). Decadal variations in the relationship between the Western Pacific subtropical high and summer heat waves in east China. *Journal of Climate*, *1*(5), 1627–1640. 10.1175/JCLI-D-18-0093.1

Lu, X., Yu, H., Ying, M., Zhao, B., Zhang, S., Lin, L., et al. (2021). Western north Pacific tropical cyclone database created by the China meteorological administration. *Advances in Atmospheric Sciences*, *38*(4), 690–699. https://doi.org/10.1007/s00376-020-0211-7

Matthews, T., Wilby, R. L., & Murphy, C. (2019). An emerging tropical cyclone–deadly heat compound hazard. *Nature Climate Change*, *9*(8), 602–606. https://doi.org/10.1038/s41558-019-0525-6

Mei, W., & Xie, S.-P. (2016). Intensification of landfalling typhoons over the northwest Pacific since the late 1970s. *Nature Geoscience*, *9*(10), 753–757. https://doi.org/10.1038/ngeo2792

Murakami, H., Delworth, T. L., Cooke, W. F., Zhao, M., Xiang, B., & Hsu, P.-C. (2020). Detected climatic change in global distribution of tropical cyclones. *Proceedings of the National Academy of Sciences*, *117*(20), 10706–10714. https://doi.org/10.1073/pnas.1922500117

Needham, H. F., Keim, B. D., & David, S. (2015). A review of tropical cyclone-generated storm surges: Global data sources, observations, and impacts. *Reviews of Geophysics*, *53*(2), 545–591. https://doi.org/10.1002/2014RG000477

Patricola, C. M., & Wehner, M. F. (2018). Anthropogenic influences on major tropical cyclone events. *Nature*, *563*(7731), 339–346. https://doi.org/10.1038/s41586-018-0673-2

Perkins-Kirkpatrick, S. E., & Lewis, S. C. (2020). Increasing trends in regional heatwaves. *Nature Communications*, *11*(1), 3357. https://doi.org/10.1038/s41467-020-16970-7

Qi, C., Wang, P., Yang, Y., Li, H., Zhang, H., Ren, L., et al. (2024). Impacts of tropical cyclone–heat wave compound events on surface ozone in eastern China: Comparison between the Yangtze river and pearl river deltas. *Atmospheric Chemistry and Physics*, *24*(20), 11775–11789. https://doi.org/10.5194/acp-24-11775-2024

Reed, K. A., & Jablonowski, C. (2011). Impact of physical parameterizations on idealized tropical cyclones in the community atmosphere model. *Geophysical Research Letters*, *38*(4), L04805. https://doi.org/10.1029/2010GL046297

Roberts, M. J., Baker, A., Ed Blockley, W., Calvert, D., Coward, A., Hewitt, H. T., et al. (2019). Description of the resolution hierarchy of the global coupled HadGEM3-GC3.1 model as used in CMIP6 HighResMIP experiments. *Geoscientific Model Development*, *12*(12), 4999–5028. https://doi.org/10.5194/gmd-12-4999-2019

Santos-Lozada, A. R., & Howard, J. T. (2018). Use of death counts from vital statistics to calculate excess deaths in Puerto Rico following hurricane Maria. *JAMA*, *320*(14), 1491–1493. https://doi.org/10.1001/jama.2018.10929

Studholme, J., Fedorov, A. V., Gulev, S. K., Emanuel, K., & Kevin, H. (2022). Poleward expansion of tropical cyclone latitudes in warming climates. *Nature Geoscience*, *15*(1), 14–28. https://doi.org/10.1038/s41561-021-00859-1

Ullrich, P. A., & Zarzycki, C. M. (2017). TempestExtremes: A framework for scale-insensitive pointwise feature tracking on unstructured grids. *Geoscientific Model Development*, *10*(3), 1069–1090. https://doi.org/10.5194/gmd-10-1069-2017

Ullrich, P. A., Zarzycki, C. M., McClenny, E. E., Pinheiro, M. C., Stansfield, A. M., & Reed, K. A. (2021). TempestExtremes v2.1: A community framework for feature detection, tracking, and analysis in large datasets. *Geoscientific Model Development*, *14*(8), 5023–5048. https://doi.org/10.5194/gmd-14-5023-2021

Utsumi, N., & Kim, H. (2022). Observed influence of anthropogenic climate change on tropical cyclone heavy rainfall. *Nature Climate Change*, *12*(5), 436–440. https://doi.org/10.1038/s41558-022-01344-2

Voldoire, A., Saint-Martin, D., Sénési, S., Decharme, B., Alias, A., Chevallier, M., et al. (2019). Evaluation of CMIP6 DECK experiments with CNRM-CM6-1. *Journal of Advances in Modeling Earth Systems*, *11*(7), 2177–2213. https://doi.org/10.1029/2019MS001683

Wang, P., Hui, P., Xue, D., & Tang, J. (2019). Future projection of heat waves over China under global warming within the CORDEX-EA-II project. *Climate Dynamics*, *53*(1–2), 957–973. https://doi.org/10.1007/s00382-019-04621-7

Wang, P., Tang, J., Sun, X., Wang, S., Wu, J., Dong, X., & Fang, J. (2017). Heat waves in China: Definitions, leading patterns, and connections to large-scale atmospheric circulation and SSTs. *Journal of Geophysical Research: Atmospheres*, *122*(20), 10679–10699. https://doi.org/10.1002/2017JD027180

Wang, P., Yang, Y., Xue, D., Qu, Y., Tang, J., Leung, L. R., & Liao, H. (2023). Increasing compound hazards of tropical cyclones and heatwaves over southeastern Coast of China under climate warming. *Journal of Climate*, *36*(7), 2243–2257. https://doi.org/10.1175/JCLI-D-22-0279.1

World Climate Research Programme. (2019). Coupled model intercomparison project phase 6 (CMIP6) [Dataset]. Retrieved from https://esgf-node.llnl.gov/projects/cmip6/

Wu, J., Chen, Y., Liao, Z., Gao, X., Zhai, P., & Hu, Y. (2022). Increasing risk from landfalling tropical cyclone-heatwave compound events to coastal and inland China. *Environmental Research Letters*, *17*(10), 105007. https://doi.org/10.1088/1748-9326/ac9747

Wu, J., & Gao, X.-J. (2013). A gridded daily observation dataset over China region and comparison with the other datasets. *Chinese Journal of Geophysics*, *56*(4), 1102–1111. https://doi.org/10.6038/cjg20130406

Xi, M., Xie, M., Gao, D., Ma, D., Luo, Y., Feng, L., et al. (2025). The impact of tropical cyclones on regional ozone pollution and its future trend in the Yangtze River Delta of China. *Atmospheric Chemistry and Physics*, *25*, 14573–14590. https://doi.org/10.5194/acp-25-14573-2025

Ying, M., Zhang, W., Yu, H., Lu, X., Feng, J., Fan, Y., et al. (2014). An overview of the China meteorological administration tropical cyclone database. *Journal of Atmospheric and Oceanic Technology*, *31*(2), 287–301. https://doi.org/10.1175/JTECH-D-12-00119.1

You, Q., Jiang, Z., Kong, L., Wu, Z., Bao, Y., Kang, S., & Pepin, N. (2017). A comparison of heat wave climatologies and trends in China based on multiple definitions. *Climate Dynamics*, *48*(11–12), 3975–3989. https://doi.org/10.1007/s00382-016-3315-0

Zhang, M., Yang, Y., Zhan, C., Zong, L., Gul, C., & Wang, M. (2024). Tropical cyclone-related heatwave episodes in the greater Bay area, China: Synoptic patterns and urban-rural disparities. *Weather and Climate Extremes*, *44*, 100656. https://doi.org/10.1016/j.wace.2024.100656

Zhao, J., Zhan, R., Wang, Y., & Xu, H. (2018). Contribution of the interdecadal Pacific oscillation to the recent abrupt decrease in tropical cyclone genesis frequency over the Western north Pacific since 1998. *Journal of Climate*, *31*(20), 8211–8224. https://doi.org/10.1175/JCLI-D-18-0202.1